


Cite this: *RSC Adv.*, 2021, 11, 3703

Received 14th November 2020  
Accepted 10th January 2021

DOI: 10.1039/d0ra09686e

rsc.li/rsc-advances

# Bis-BODIPY linked-triazole based on catechol core for selective dual detection of Ag<sup>+</sup> and Hg<sup>2+</sup>†

Worakrit Saiyasombat<sup>a</sup> and Supavadee Kiatisevi<sup>b</sup>  \*<sup>ab</sup>

Herein, we introduced a new chemosensor, bis-BODIPY linked-triazole based on catechol (BODIPY-OO) prepared by bridging two units of BODIPY fluorophore/triazole binding group with a catechol unit. A solution of this compound displayed 4- and 2-fold enhancements in fluorescence intensity after adding a mole equivalent amount of Ag<sup>+</sup> and Hg<sup>2+</sup> ions in methanol media, respectively. <sup>1</sup>H NMR titrations of BODIPY-OO with Ag<sup>+</sup> and Hg<sup>2+</sup> suggested that the triazole was involved in the recognition process. BODIPY-OO showed high sensitivity toward Ag<sup>+</sup> and Hg<sup>2+</sup> over other metal ions with detection limits of 0.45 μM and 1 μM, respectively. It can also distinguish Hg<sup>2+</sup> from Ag<sup>+</sup> by addition of an EDTA. This compound can therefore be employed as practical fluorescent probe for monitoring the presence of Ag<sup>+</sup> and Hg<sup>2+</sup> ions.

## Introduction

Since toxicity of heavy and transition metal ions affects biological and environmental systems, it is highly desirable to develop sensing probes to monitor and quantify these ions.<sup>1–3</sup> Specifically, mercury is used in various industries such as pharmaceuticals, batteries, semi-conductors, agriculture, and paper industry.<sup>4</sup> It is also widely used in dentistry and scientific research as amalgam.<sup>5,6</sup> The Agency for Toxic Substances and Disease Registry (ATSDR) has ranked mercury as the third of most toxic substances.<sup>7</sup> Its widespread use leads to the release and accumulation of mercury in general environment.<sup>8</sup> Humans are exposed to mercury mainly through consumption of contaminated food, inhalation, and even through the skin causing gut lining and kidney damage, pneumonitis and disorder of many parts of the brain and peripheral nervous system.<sup>6</sup> In addition to mercury, silver has been extensively used by many industrial applications such as in photovoltaics, photography, jewelry and silverware production.<sup>9,10</sup> Silver has also long been known for its antimicrobial properties and has been used for years in the medical field.<sup>11</sup> Although it shows a low level of toxicity to human,<sup>12</sup> high levels of the silver ion can inhibit glutathione (GSH), markers, and antioxidant enzymes.<sup>13</sup> Silver also reduces superoxide dismutase (SOD) levels causing an oxidative stress and production of reactive oxygen species (ROS). In addition,

prolonged exposure to silver may lead to irreversible discoloration of skin or eyes, *i.e.* argyria or argyrosis.<sup>14</sup>

There are a lot of analytical techniques for mercury and silver determination such as atomic absorption spectrometry (AAS),<sup>15</sup> inductively coupled plasma mass spectroscopy (ICP-MS),<sup>16</sup> inductively coupled plasma-atomic emission spectroscopy (ICP-AES),<sup>17</sup> and electrochemical methods.<sup>18</sup> However, these methods are time-consuming and require sophisticated instrumentation. A simple, inexpensive, and efficient alternative is fluorescent sensor where binding of the analyte leads to a change in fluorescence which requires only cheap routine spectrometers.<sup>19,20</sup> A good fluorescent sensor should not only be sensitive and selective but also allows real-time monitoring of targeted metal ions with low response time.<sup>21,22</sup>

Small-molecule fluorescent chemosensors are usually composed of a fluorophore and a chelating or recognition unit. The fluorophores with excellent optical properties, such as coumarin,<sup>23</sup> fluorescein,<sup>24</sup> rhodamine<sup>25</sup> and BODIPY<sup>26</sup> provide highly sensitive fluorescent chemosensors. Among these, BODIPY derivatives show great potentials owing to their outstanding photophysical properties, *i.e.* spectral bands tunable along the whole visible spectrum, high molar absorption coefficients (>80 000 cm<sup>−1</sup> M<sup>−1</sup>), and high fluorescence quantum yields.<sup>27,28</sup> Owing to their soft character, nitrogen heterocyclic systems, *e.g.* pyridine,<sup>29</sup> quinoline,<sup>30</sup> imidazole,<sup>31</sup> and triazole<sup>32</sup> are mostly used as recognition units for various metal ions and tend to react with soft acids such as mercury and silver ions. The triazole ring has emerged as an exciting moiety in the study of sensors. This stems from a robust and green protocol for the synthesis of triazole derivatives.<sup>33</sup> In addition to metal sensors, triazole is extensively used in the synthesis of catalyst,<sup>34</sup> dendrimers,<sup>35</sup> biomolecule conjugates,<sup>36</sup> and metal organic frameworks.<sup>37</sup>

BODIPY–triazole combinations were reported as fluorescent chemosensors for the detection of metal ions, *e.g.* Hg<sup>2+</sup>,<sup>38</sup> Cu<sup>2+</sup>,<sup>39</sup>

<sup>a</sup>Department of Chemistry, Center of Excellence for Innovation in Chemistry (PERCH-CIC), Faculty of Science, Mahidol University, Rama VI Rd, Rajthevi, Bangkok 10400, Thailand. E-mail: supavadee.mon@mahidol.edu; Fax: +66-2-354-7151; Tel: +66-2-201-5150

<sup>b</sup>Center of Sustainable Energy and Green Materials, Faculty of Science, Mahidol University, Salaya, Putthamonthon, Nakhon Pathom 73170, Thailand

† Electronic supplementary information (ESI) available. See DOI: 10.1039/d0ra09686e



$\text{Al}^{3+}$ ,<sup>40</sup> and  $\text{Ag}^+$ .<sup>41</sup> This construction pattern offers following advantages: (i) click reaction affords triazoles in high yields with simple synthetic protocols; (ii) two triazole units acting as a chelation pocket can efficiently capture metal ions; (iii) the presence of two BODIPY fluorophore units improves the sensitivity of detection; and (iv) optical properties of the triazole containing BODIPY are easily tuned by modifications to spacers and chelating moieties.<sup>38–41</sup> However, there are no reports on using such a fluorescent chemosensor template for recognizing multiple target ions which has the advantages of being cost-effective and highly efficient. In addition, the fluorescent chemosensors that can serve as bifunctional detection of mercury and silver ion are still rare.<sup>42–45</sup> Herein, we designed and synthesized a new fluorescent sensor (**BODIPY-OO**) composed of two units of azido-BODIPY (**2**) and one unit of 1,2-bis(prop-2-yn-1-yloxy)benzene (**3**) covalently linked by an alkyne–azide click chemistry approach (Scheme 1). Its spectroscopic properties were investigated. **BODIPY-OO** presented “turn-on” fluorescence behaviors toward the silver and mercury ions over other interfering metal ions.

## Experimental

### Materials and equipment

Unless otherwise noted, all chemicals are of analytical reagent grade obtained from commercial suppliers and are used without further purification. Dichloromethane ( $\text{CH}_2\text{Cl}_2$ ) was distilled from calcium hydride and stored under 4 Å molecular sieves. Water utilized in the analysis processes was obtained from Millipore system and deionized prior to use. Azido BODIPY **2** was synthesized following literature procedures.<sup>47</sup> Alkyne **3** was prepared by conventional propargylation reaction using propargyl bromide and  $\text{K}_2\text{CO}_3$ . Column chromatography was performed on Merck silica gel 60 (70–230 mesh).  $^1\text{H}$  and  $^{13}\text{C}$  NMR spectra were recorded on Bruker Ascend™ 400 MHz spectrometers. The chemical shifts ( $\delta$ ) and coupling constants ( $J$ ) are reported in parts per million (ppm) and Hertz (Hz), respectively. Tetramethylsilane (TMS) or residual non-deuterated solvents are used as internal reference materials in

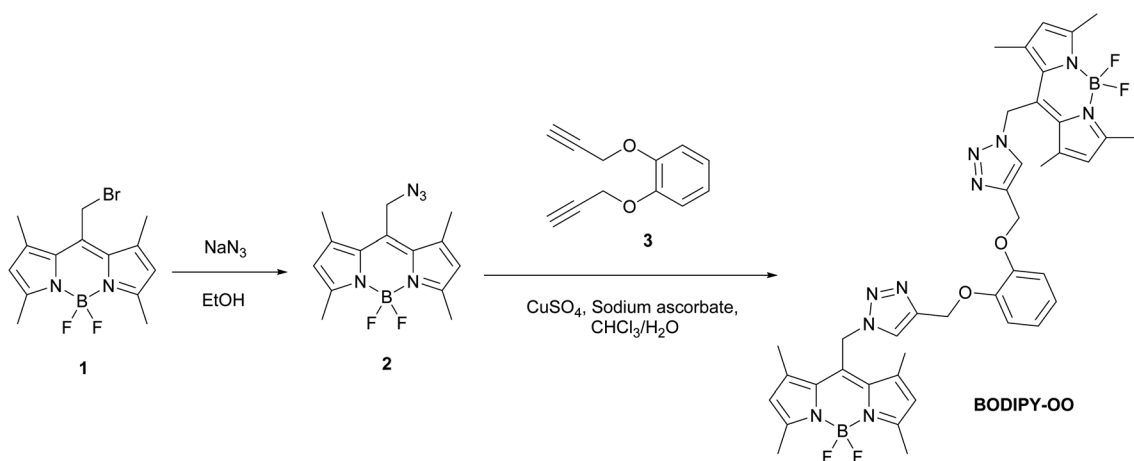
$^1\text{H}$  NMR experiments. HRMS spectra were recorded on a HR-TOF-MS Micromass model VQ-TOF2. UV-Vis and fluorescence spectrometers were monitored on a UV-2600 (Shimadzu) and a FluoroMax® Plus (HORIBA), respectively.

### Syntheses

**Azido-BODIPY (2).** **1** (100 mg, 0.29 mmol) was dissolved in ethanol (50 mL). To this mixture, sodium azide (89.0 mg, 1.37 mmol) was added. The round-bottom flask was then wrapped with aluminum foil and placed under argon. The reaction was stirred at 40 °C for 18 h. The solvent was removed under reduced pressure. The crude mixture was dissolved in ethyl acetate, washed with water, and dried over anhydrous  $\text{Na}_2\text{SO}_4$ . After removal of the organic solvent, the crude product was then purified on a silica gel column using an elution of 50%  $\text{CH}_2\text{Cl}_2$  in hexane to afford an orange-red solid in 80% yield (70 mg).  $^1\text{H}$  NMR (400 MHz,  $\text{CDCl}_3$ ):  $\delta$  6.10 (s, 2H), 4.60 (s, 2H), 2.53 (s, 6H), 2.46 (s, 6H).  $^{13}\text{C}$  NMR (100 MHz,  $\text{CDCl}_3$ ):  $\delta$  156.81, 141.36, 133.23, 132.18, 122.70, 44.78, 16.23, 14.83. HRMS (ESI)  $m/z$ : calcd for  $\text{C}_{14}\text{H}_{16}\text{BF}_2\text{N}_5\text{Na}$  [ $\text{M} + \text{Na}$ ]<sup>+</sup>, 326.1359; found, 326.1360.

**1,2-Bis(prop-2-yn-1-yloxy)benzene (3).** Propargyl bromide (294 mg, 2 mmol) and  $\text{K}_2\text{CO}_3$  (276 mg, 2 mmol) were added to a solution of *o*-dihydroxybenzene (100 mg, 0.91 mmol) in acetone (5 mL). The mixture was heated to refluxing under argon for 18 h. After removal of solvent, the crude product was extracted with ethyl acetate, washed with water, and dried over anhydrous  $\text{Na}_2\text{SO}_4$ . It was then evaporated under reduced pressure and purified by chromatography on silica gel to afford 122 mg (85%) of **3** as a pale-yellow oil.  $^1\text{H}$  NMR (400 MHz,  $\text{CDCl}_3$ ):  $\delta$  7.08–7.05 (m, 2H), 7.01–6.97 (m, 2H), 4.76 (d,  $J$  = 2.2 Hz, 4H), 2.51 (t,  $J$  = 2.2 Hz, 2H).  $^{13}\text{C}$  NMR (100 MHz,  $\text{CDCl}_3$ ):  $\delta$  147.79, 122.32, 115.33, 78.75, 75.87, 57.06. HRMS (ESI)  $m/z$ : calcd for  $\text{C}_{12}\text{H}_{10}\text{NaO}_2$  [ $\text{M} + \text{Na}$ ]<sup>+</sup>, 209.0573; found, 209.0572.

**Sensor (BODIPY-OO).** In a Schlenk tube, **3** (20 mg, 0.10 mmol) and **2** (65 mg, 0.21 mmol) were stirred in 3 mL of  $\text{CHCl}_3$  at room temperature under argon. To the solution mixture were added 20 mol% of  $\text{CuSO}_4 \cdot 5\text{H}_2\text{O}$  and 40 mol% of sodium ascorbate dissolved in deionized water. The solution was stirred



Scheme 1 BODIPY-OO synthesis.



for 18 h, poured into water and extracted with  $\text{CH}_2\text{Cl}_2$ . The combined organic layers were washed with water and dried over anhydrous  $\text{Na}_2\text{SO}_4$ . After solvent evaporation, the crude product was further purified by column chromatography with a gradient eluent (25%, 50%, and 100% EtOAc in hexane). **BODIPY-OO** was obtained as a red solid in 66% yield (52 mg, 0.066 mmol).  $^1\text{H}$  NMR (400 MHz,  $\text{CDCl}_3$ ):  $\delta$  7.57 (s, 2H), 6.96–6.92 (m, 2H), 6.86–6.82 (m, 2H), 6.08 (s, 4H), 5.77 (s, 4H), 5.13 (s, 4H), 2.53 (s, 12H), 2.15 (s, 12H).  $^{13}\text{C}$  NMR (100 MHz,  $\text{CDCl}_3$ ):  $\delta$  157.81, 148.55, 144.49, 141.56, 132.36, 129.95, 123.16, 122.57, 122.23, 116.65, 63.56, 45.74, 15.82, 14.89.  $^{11}\text{B}$  NMR (128 MHz,  $\text{CDCl}_3$ ):  $\delta$  -0.45 (t,  $J_{\text{BF}}$  = 33.3 Hz).  $^{19}\text{F}$  NMR (377 MHz,  $\text{CDCl}_3$ ):  $\delta$  -145.9 (q,  $J_{\text{FB}}$  = 33.9 Hz). HRMS (ESI)  $m/z$ : calcd for  $\text{C}_{40}\text{H}_{42}\text{B}_2\text{F}_4\text{N}_{10}\text{NaO}_2$  [ $\text{M} + \text{Na}$ ] $^+$ , 815.3507; found, 815.3509.

### Measurements of UV-Vis and fluorescence spectra

In UV-Vis studies, all metal salts including  $\text{NaNO}_3$ ,  $\text{Mg}(\text{NO}_3)_2 \cdot 6\text{H}_2\text{O}$ ,  $\text{Fe}(\text{NO}_3)_3 \cdot 9\text{H}_2\text{O}$ ,  $\text{Co}(\text{NO}_3)_2 \cdot 6\text{H}_2\text{O}$ ,  $\text{Ni}(\text{NO}_3)_2 \cdot 6\text{H}_2\text{O}$ ,  $\text{Cu}(\text{NO}_3)_2 \cdot 3\text{H}_2\text{O}$ ,  $\text{Zn}(\text{NO}_3)_2 \cdot 6\text{H}_2\text{O}$ ,  $\text{Cd}(\text{NO}_3)_2 \cdot 4\text{H}_2\text{O}$ ,  $\text{AgNO}_3$ ,  $\text{Pb}(\text{NO}_3)_2$ ,  $\text{Hg}(\text{NO}_3)_2$ , and  $\text{Cr}(\text{NO}_3)_3 \cdot 9\text{H}_2\text{O}$  were prepared in deionized water to get  $10^{-2}$  M stock solutions. Solutions of the **BODIPY-OO** sensor (5  $\mu\text{M}$ ) were prepared in methanol. Test solutions were prepared by mixing 30  $\mu\text{L}$  of each metal stock solution with 3 mL of the sensor solution in a quartz cuvette (path length = 1 cm). In fluorescence studies, solutions of sensor (0.5  $\mu\text{M}$ ) were prepared in methanol. Test solutions were prepared by mixing 3  $\mu\text{L}$  of the metal stock solution with 3 mL of the sensor solution in a quartz cuvette (path length = 1 cm). The excitation wavelength was set at 470 nm and the emission wavelength range was 500–700 nm. The slit width was 3.0 nm for both excitation and emission experiments.

### Fluorescence titrations

A solution (1  $\mu\text{M}$ ) of the **BODIPY-OO** sensor was prepared in methanol. 3–30  $\mu\text{L}$  of a  $10^{-3}$  M stock solution of  $\text{Hg}(\text{NO}_3)_2$  or  $\text{AgNO}_3$  were added to 3 mL of the sensor solution. After mixing them in a quartz cuvette (path length = 1 cm) for a few seconds, fluorescence spectra were taken at room temperature.

### Competition experiments

A solution of the sensor **BODIPY-OO** (0.5  $\mu\text{M}$ ) was prepared in MeOH. Stock solutions ( $10^{-2}$  M) of various metal ions were prepared. 3  $\mu\text{L}$  of each metal solution was added to 3 mL of the sensor solution to make 20 equiv. of the metal ion. 3  $\mu\text{L}$  of the  $\text{Hg}^{2+}$  or  $\text{Ag}^+$  solution was then added into the mixed solution to get 20 equiv. of  $\text{Hg}^{2+}$  or  $\text{Ag}^+$ . After mixing them for a few seconds, fluorescence spectra were taken at room temperature.

### $^1\text{H}$ NMR titrations

A solution of the sensor **BODIPY-OO** (1.00 mg, 0.001 mmol) in  $\text{DMSO}-d_6$  was prepared. 2–6  $\mu\text{L}$  of 0.32 M  $\text{AgNO}_3$  solution in  $\text{DMSO}-d_6$  was added to the sensor solution to make a 1 : 0.5, 1 : 1, and 1 : 1.5 molar ratios of ligand to metal. After shaking them for a minute,  $^1\text{H}$  NMR spectra were taken at room temperature. For  $\text{Hg}^{2+}$ , the same procedure was performed but  $\text{HgCl}_2$  and acetone- $d_6$  were used as mercury source and solvent, respectively.

### Computational calculation

The structure and electronic properties of **BODIPY-OO**, **BODIPY-OO-Ag $^+$**  and **BODIPY-OO-Hg $^{2+}$**  were calculated using density functional theory (DFT) and its extension to the time-dependent formulation (TDDFT) as implemented in Gaussian 09 package.<sup>48</sup> The ground state structures were optimized in gas-phase with the B3LYP<sup>49,50</sup> functional and 6-31G(d) basis set<sup>51,52</sup> for the main group elements and LANL2DZ effective core potential (ECP)<sup>53–55</sup> for Hg and Ag atoms. TDDFT calculations of the 10 lowest singlet–singlet transitions were carried out on the optimized ground state geometries using CAM-B3LYP<sup>56</sup>/6-31G(d), and CAM-B3LYP/GENECP for the free ligand and its complexes, respectively, adopting the conductor-like polarization (CPCM)<sup>57,58</sup> model for the solvent (methanol) effect. Molecular orbitals were plotted using Avogadro program.<sup>59,60</sup>

## Results and discussion

### Construction of BODIPY-OO fluorescent platform

**BODIPY-OO** designed as a sensor for detection of multiple metal ions contains a catechol moiety and two triazole units in the binding core. Copper-catalyzed azide–alkyne cycloaddition (CuAAC) was used to synthesize **BODIPY-OO** as depicted in Scheme 1. Azido-BODIPY **2** was obtained by azidation of its bromo analog **1**, while the terminal bisalkyne **3** was prepared by the propargylation reaction of catechol. The click reaction between bisalkyne-terminated catechol ether and azido-terminated BODIPY in the presence of  $\text{CuSO}_4$  and sodium ascorbate in  $\text{CHCl}_3/\text{H}_2\text{O}$  media resulted in the formation of the target compound in 66% yield.

**BODIPY-OO** was purified by column chromatography and characterized by  $^1\text{H}$ ,  $^{13}\text{C}$ ,  $^{11}\text{B}$ ,  $^{19}\text{F}$  NMR, and FTIR spectroscopy, and HRMS spectrometry. The triazole protons of **BODIPY-OO** in the  $^1\text{H}$  NMR spectrum resonated at  $\delta$  7.57 ppm as a singlet. Aromatic protons of the catechol unit appeared over the range of  $\delta$  6.96–6.92 ppm and 6.86–6.82 ppm whereas signals at  $\delta$  6.08 ppm corresponded to protons at 2,6 positions of the BODIPY core.  $^1\text{H}$  chemical shifts of methylene protons attached to the BODIPY core and those attached to oxygen atoms were observed at 5.77 and 5.13 ppm, respectively. Methyl protons of the BODIPY units

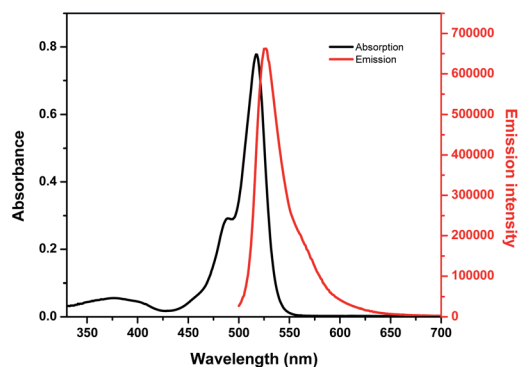


Fig. 1 Absorption and emission spectra of **BODIPY-OO** (5  $\mu\text{M}$ ) in MeOH ( $\lambda_{\text{ex}}$  = 470 nm, slit: 3).



Table 1 Photophysical properties of BODIPY-OO and its complexes

| Compound                    | $\lambda_{\text{abs}}^{\text{max}}$ (nm) | $\epsilon$ ( $\text{M}^{-1} \text{cm}^{-1}$ ) | $\lambda_{\text{em}}^{\text{max}}$ (nm) | $\Phi_{\text{F}}^a$ | Binding constant ( $\text{M}^{-1}$ ) |
|-----------------------------|--|---|---|---------------------|--------------------------------------|
| BODIPY-OO                   | 517                                      | $1.5 \times 10^5$                             | 527                                     | 0.06                | —                                    |
| BODIPY-OO- $\text{Ag}^+$    | 517                                      | $1.8 \times 10^5$                             | 527                                     | 0.22                | $1.56 \times 10^5$                   |
| BODIPY-OO- $\text{Hg}^{2+}$ | 521                                      | $1.6 \times 10^5$                             | 531                                     | 0.12                | $1.41 \times 10^5$                   |

<sup>a</sup> Relative to fluorescein in 0.1 N NaOH ( $\Phi_{\text{F}} = 0.95$ ).<sup>46</sup>

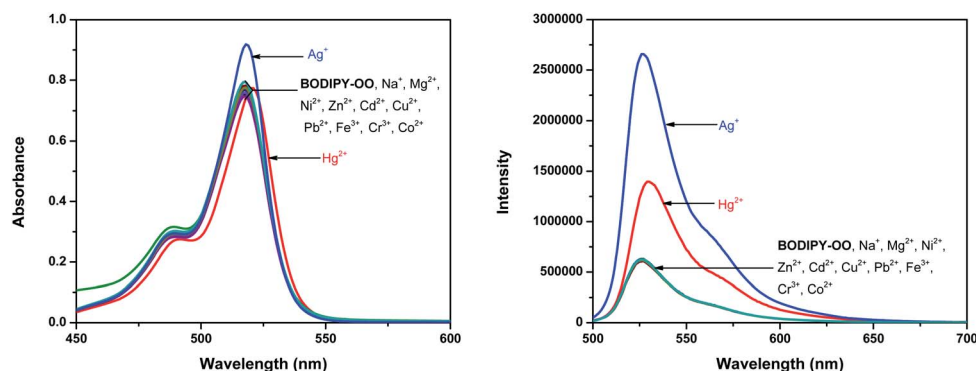


Fig. 2 Left: absorption spectra of BODIPY-OO (5  $\mu\text{M}$ ) in the presence of various metal ions (20 equiv.) in MeOH. Right: emission spectra of BODIPY-OO (0.5  $\mu\text{M}$ ) in the presence of various metal ions (20 equiv.) in MeOH ( $\lambda_{\text{ex}} = 470 \text{ nm}$ , slit: 3).

resonated at  $\delta$  2.53 and 2.15 ppm. In addition, the  $^{11}\text{B}$  and  $^{19}\text{F}$  NMR spectra of BODIPY-OO exhibited a typical triplet ( $^{11}\text{B}$ ) and quartet ( $^{19}\text{F}$ ) due to B-F coupling (Fig. S15 and S16, ESI†).

### Sensing behaviors of BODIPY-OO

Optical properties of BODIPY-OO in methanol were first studied by absorption and emission spectroscopic methods (Fig. 1). The absorption spectrum displays three typical bands in the visible region: an intense main band at 517 nm attributed to typical  $\pi$ - $\pi^*$  transition ( $S_0 \rightarrow S_1$ ) of the BODIPY units; a small shoulder on the high-energy side of the main band at 489 nm ascribed to the 0-1 vibrational transition; and a weaker broad band at 375 nm which can be assigned to  $S_0 \rightarrow S_n$  ( $n \geq 2$ ) transitions.<sup>64</sup> The fluorescence spectrum of BODIPY-OO was obtained after excitation within the spectral region of the absorption maximum which showed a single green fluorescence peak at 527 nm. BODIPY-OO has a fluorescence quantum yield ( $\Phi_{\text{F}}$ ) of 0.06 relative to fluorescein ( $\Phi_{\text{F}} = 0.95$  in 0.1 N NaOH) as shown in Table 1.<sup>46</sup>

Our investigation began with the evaluation of the optical behaviors of BODIPY-OO in response to the addition (20 equiv.) of different ions such as  $\text{Na}^+$ ,  $\text{Mg}^{2+}$ ,  $\text{Fe}^{3+}$ ,  $\text{Co}^{2+}$ ,  $\text{Ni}^{2+}$ ,  $\text{Cu}^{2+}$ ,  $\text{Zn}^{2+}$ ,  $\text{Cd}^{2+}$ ,  $\text{Ag}^+$ ,  $\text{Pb}^{2+}$ ,  $\text{Hg}^{2+}$ , and  $\text{Cr}^{3+}$ . Fluorescence and UV-visible spectra indicated that BODIPY-OO was only sensitive to the  $\text{Hg}^{2+}$  and  $\text{Ag}^+$  ions (Fig. 2). Both ions increased the fluorescence intensity of the probe BODIPY-OO, when excited with  $\lambda_{\text{ex}} = 470 \text{ nm}$ . The addition of  $\text{Hg}^{2+}$  to BODIPY-OO resulted in a small redshift of the absorption spectrum whereas the emission curves displayed a 2-fold enhancement of the fluorescence intensity at 531 nm with  $\Phi_{\text{F}}$  of 0.12. In contrast, the addition of  $\text{Ag}^+$  led to a hyperchromic shift with molar extinction coefficient

increasing from  $1.5 \times 10^5 \text{ M}^{-1} \text{cm}^{-1}$  (BODIPY-OO) to  $1.8 \times 10^5 \text{ M}^{-1} \text{cm}^{-1}$  (BODIPY-OO- $\text{Ag}^+$ ). Notably, the chelation of BODIPY-OO with the  $\text{Ag}^+$  ion increased the fluorescence intensity at 527 nm of ca. 4-fold ( $\Phi_{\text{F}} = 0.22$ ) with respect to BODIPY-OO ( $\Phi_{\text{F}} = 0.06$ ). As shown in Fig. 3, our probe exhibited turn-on fluorescence toward  $\text{Ag}^+$  and  $\text{Hg}^{2+}$  likely as a result of chelation-enhanced fluorescence (CHEF) effect<sup>62,63</sup> that is caused by the restriction of the intramolecular rotations in BODIPY-OO.<sup>64</sup> The effect also decreases the non-radiative decay of the excited state. Notably, these results are different from the previously reported bifunctional probes for  $\text{Ag}^+$  and  $\text{Hg}^{2+}$  which mainly involved turn-off processes due to heavy atom effect and spin-orbit coupling (Table S1, ESI†).<sup>42,65-67</sup>

### Fluorescence titrations of BODIPY-OO with different ion concentrations

To further investigate the sensing behaviors of BODIPY-OO toward various concentrations of  $\text{Ag}^+$  and  $\text{Hg}^{2+}$ , the fluorescence

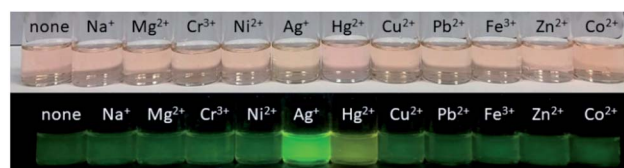


Fig. 3 Top: photograph of BODIPY-OO (5  $\mu\text{M}$ ) toward tested metal ions (20 equiv.) in MeOH. Bottom: fluorogenic responses of BODIPY-OO (5  $\mu\text{M}$ ) toward tested metal ions (20 equiv.) in MeOH under UV light ( $\lambda_{\text{ex}} = 365 \text{ nm}$ ).





titration experiment was performed. The plots of fluorescence intensity as a function of the  $\text{Ag}^+$  and  $\text{Hg}^{2+}$  concentrations are shown in Fig. 4a and b, respectively. Upon sequential addition of  $\text{Ag}^+$  (0–10 equiv.) to the solution of **BODIPY-OO**, the fluorescence intensity of **BODIPY-OO** gradually increased and became saturated when the amount of  $\text{Ag}^+$  reached 9 equivalents when excited with  $\lambda_{\text{ex}} = 470$  nm. The detection limit of **BODIPY-OO** for the  $\text{Ag}^+$  detection was estimated to be  $0.45 \mu\text{M}$  using the

equation:  $\text{LOD} = 3\sigma/S$ ,<sup>68</sup> where  $S$  is the slope of the curve between the fluorescence intensities of the probe **BODIPY-OO** and the concentrations of  $\text{Ag}^+$ , and  $\sigma$  is the standard deviation of four replicate measurements of the zero level ( $\sigma$ ) (Fig. S1b, ESI†). After addition of increasing concentrations of  $\text{Hg}^{2+}$  (0–15 equiv.) to the solution of **BODIPY-OO**, the fluorescence intensity gradually increased, and eventually reached the plateau when the amount of  $\text{Hg}^{2+}$  reached 9 equivalents. Furthermore, the emission peak

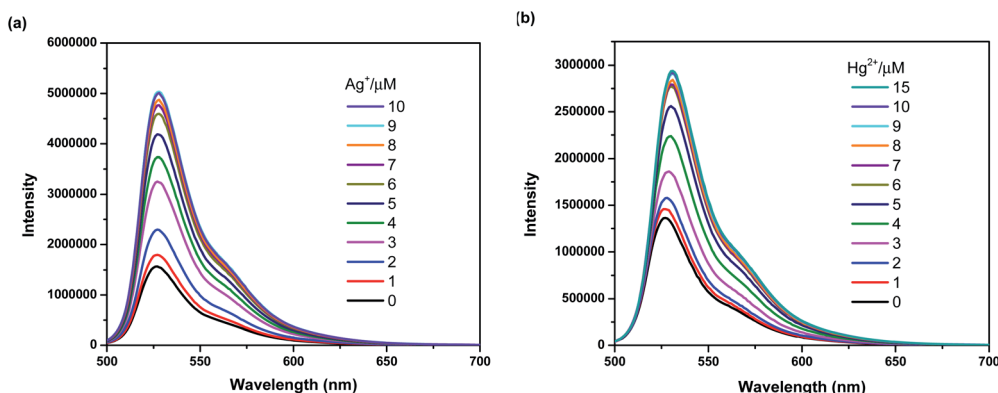


Fig. 4 (a) Fluorescence spectra of **BODIPY-OO** ( $1 \mu\text{M}$ ) with  $\text{Ag}^+$  in MeOH ( $\lambda_{\text{ex}} = 470$  nm, slit: 3). (b) Fluorescence spectra of **BODIPY-OO** ( $1 \mu\text{M}$ ) with  $\text{Hg}^{2+}$  in MeOH ( $\lambda_{\text{ex}} = 470$  nm, slit: 3).

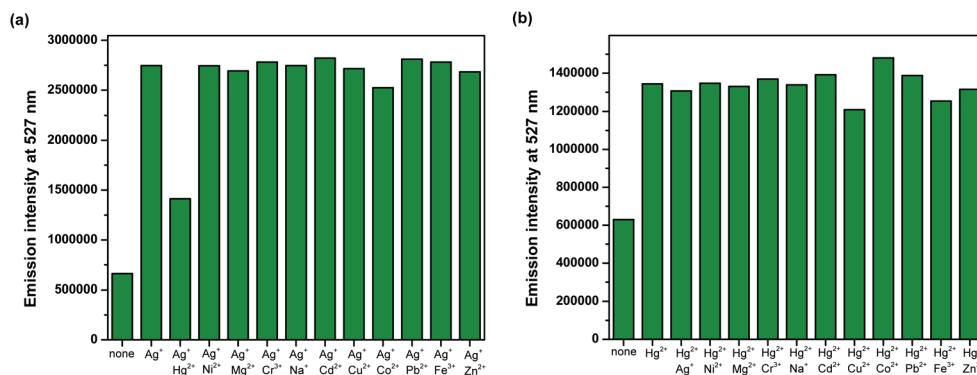


Fig. 5 Competitive selectivity of: (a) **BODIPY-OO** ( $0.5 \mu\text{M}$ ) toward  $\text{Ag}^+$  (10 equiv.) with other metal ions, and (b) **BODIPY-OO** ( $0.5 \mu\text{M}$ ) toward  $\text{Hg}^{2+}$  (10 equiv.) with other metal ions.

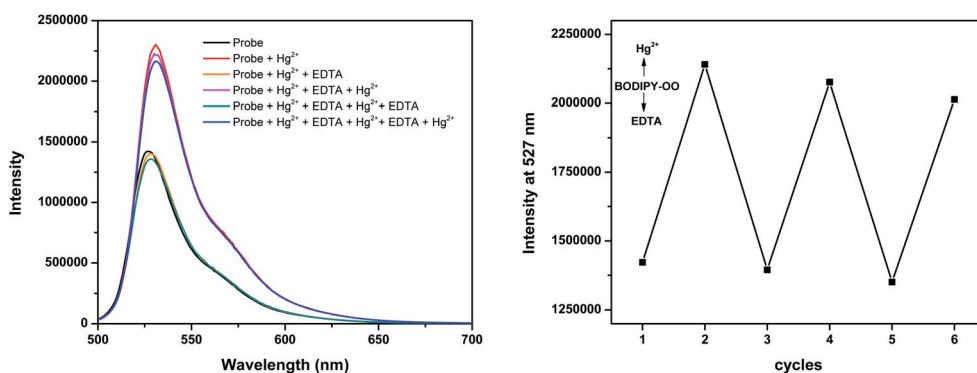


Fig. 6 Fluorescence spectral changes of **BODIPY-OO** ( $1 \mu\text{M}$ ) after the sequential addition of  $\text{Hg}^{2+}$  and EDTA.

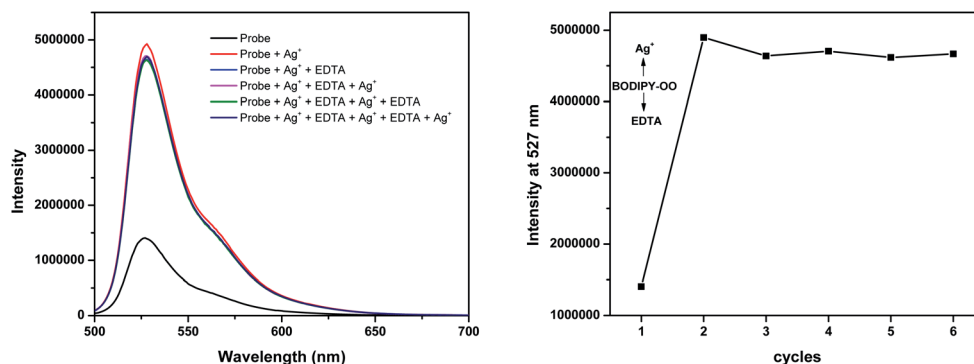


Fig. 7 Fluorescence spectral changes of BODIPY-OO (1  $\mu\text{M}$ ) after the sequential addition of  $\text{Ag}^+$  and EDTA.

gradually redshifted from 527 nm to 531 nm. According to the fluorescence titration experiment, the detection limit of BODIPY-OO for the  $\text{Hg}^{2+}$  detection was 1  $\mu\text{M}$  (Fig. S2b, ESI†).

To obtain further insight into the binding characteristics of the  $\text{Ag}^+$  and  $\text{Hg}^{2+}$  ions with BODIPY-OO, Job plot analysis was carried out using fluorescence experiments in the presence of various molar fractions of  $\text{Ag}^+$  and  $\text{Hg}^{2+}$ , respectively (Fig. S3 and S4, ESI†). A maximum emission was observed when the molar fraction of each metal ion reached the value of 0.5, indicating the formation of a 1 : 1 binding stoichiometry of both interactions between BODIPY-OO and  $\text{Ag}^+$ , and between BODIPY-OO and  $\text{Hg}^{2+}$ . In addition, association constant ( $K_a$ ) of BODIPY-OO with  $\text{Ag}^+$  was

calculated to be  $1.56 \times 10^5 \text{ M}^{-1}$  using the Benesi-Hildebrand equation<sup>69</sup> (Fig. S5, ESI†) and  $K_a$  of BODIPY-OO with  $\text{Hg}^{2+}$  was calculated to be  $1.41 \times 10^5 \text{ M}^{-1}$  (Fig. S6, ESI†).

### Interference of other metal ions

Competition experiments were conducted to investigate high selectivity toward specific analytes over other competitive species by adding 10 equiv. of either  $\text{Ag}^+$  or  $\text{Hg}^{2+}$  to the solution of BODIPY-OO in the presence of other common metal ions such as  $\text{Na}^+$ ,  $\text{Mg}^{2+}$ ,  $\text{Fe}^{3+}$ ,  $\text{Co}^{2+}$ ,  $\text{Ni}^{2+}$ ,  $\text{Cu}^{2+}$ ,  $\text{Zn}^{2+}$ ,  $\text{Cd}^{2+}$ ,  $\text{Ag}^+$ ,  $\text{Pb}^{2+}$ ,  $\text{Hg}^{2+}$ , and  $\text{Cr}^{3+}$  (20 equiv.). Fig. 5a clearly revealed no changes in the fluorescence intensity of the BODIPY-OO- $\text{Ag}^+$  complex upon

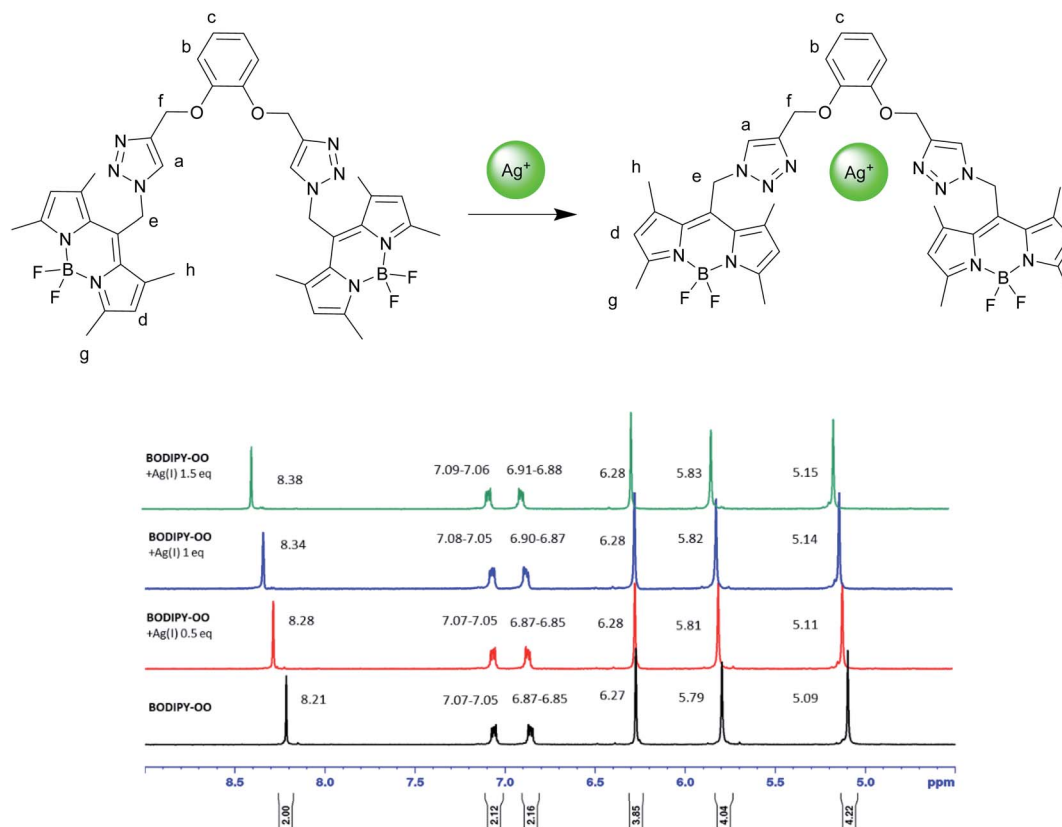


Fig. 8 Partial  $^1\text{H}$  NMR titration spectra of BODIPY-OO in  $\text{DMSO-d}_6$  upon addition of  $\text{Ag}^+$  in various amounts.



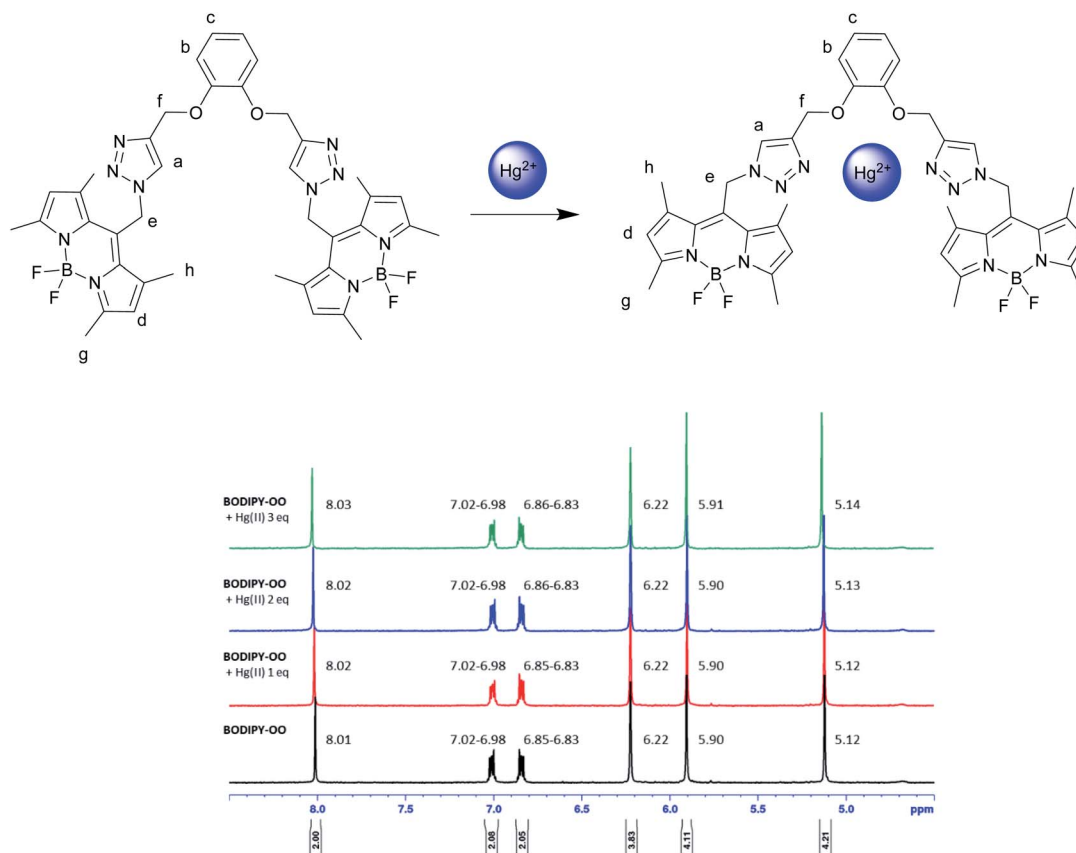


Fig. 9 Partial  $^1\text{H}$  NMR titration spectra of **BODIPY-OO** in acetone- $\text{d}_6$  upon addition of  $\text{Hg}^{2+}$  in various amounts.

addition of other metal ions with the exception of  $\text{Hg}^{2+}$ . The addition of  $\text{Hg}^{2+}$  substantially perturbed the fluorescence emission of **BODIPY-OO- $\text{Ag}^+$**  as it reduced about a half of the initial fluorescence intensity. This result implies that the  $\text{Hg}^{2+}$  ion can interfere the binding between **BODIPY-OO** and the  $\text{Ag}^+$  ion. A possible factor that affects the higher affinity of the  $\text{Hg}^{2+}$  ion as compared to  $\text{Ag}^+$  toward the receptor is the smaller ionic diameter ( $\text{Hg}^{2+}$ , 2.0 Å;  $\text{Ag}^+$ , 2.3 Å).<sup>70</sup> Based on the interference experiment for the **BODIPY-OO- $\text{Hg}^{2+}$**  complex, no significant changes occurred for the contact with the other ions (20 equiv.). As shown in Fig. 5b, the specific recognition of  $\text{Hg}^{2+}$  by **BODIPY-OO** was observed. When other interfering metal ions were added, there was no interference in the detection of  $\text{Hg}^{2+}$  from most of the metal ions.

The response behavior of **BODIPY-OO** toward the  $\text{Ag}^+$  and  $\text{Hg}^{2+}$  ions in terms of the binding ability and reversibility was further determined to discriminate the  $\text{Ag}^+$  from the  $\text{Hg}^{2+}$ . The discriminative experiment was performed using ethylenediamine tetraacetic acid (EDTA) calcium disodium salt. The addition of EDTA to a solution of **BODIPY-OO- $\text{Hg}^{2+}$**  led to an immediate decrease in the fluorescence intensity (Fig. 6). The intensity can be revived by the addition of  $\text{Hg}^{2+}$ . It was also found that the sequentially alternative addition of  $\text{Hg}^{2+}$  and EDTA resulted in the reversible emission changes even after several cycles. These results suggested a potential of the probe to be recyclable simply through treatment with a proper reagent such as EDTA. In contrast, the emission changes were not observed for the

**BODIPY-OO- $\text{Ag}^+$**  complex after the addition of EDTA, (Fig. 7). In other words, the complexation reaction of **BODIPY-OO** with the  $\text{Ag}^+$  ion was irreversible. This is because EDTA is a good chelating agent for di- and trivalent metal ions and can be seen from the greater formation constant ( $K_f$ ) for the  $\text{Hg}^{2+}$ -EDTA complex ( $\log(K_f) = 21.5$ ) when compared with the  $\text{Ag}^+$ -EDTA complex ( $\log(K_f) = 7.20$ ).<sup>71</sup> Therefore, the addition of EDTA could assist to distinguish **BODIPY-OO- $\text{Hg}^{2+}$**  from **BODIPY-OO- $\text{Ag}^+$** .

#### $^1\text{H}$ -NMR titration for **BODIPY-OO** with $\text{Ag}^+$ and $\text{Hg}^{2+}$

To understand complexation of **BODIPY-OO** with the  $\text{Ag}^+$  and  $\text{Hg}^{2+}$  ions,  $^1\text{H}$  NMR titrations were performed. Fig. 8 shows  $^1\text{H}$  NMR spectra of **BODIPY-OO** recorded in  $\text{DMSO-}d_6$  with different concentrations of  $\text{Ag}^+$  ranging from 0 to 1.5 equivalents. It was observed that the triazole ( $\text{H}_a$ ) and methylene protons ( $\text{H}_e$  and  $\text{H}_f$ ) at  $\delta$  8.21, 5.79, and 5.09 ppm were obviously downfield shifted to  $\delta$  8.38, 5.83, and 5.15 ppm, respectively, upon increasing concentrations of the  $\text{Ag}^+$ . The downfield shift of the triazole and methylene protons may arise from the interaction of  $\text{Ag}^+$  with the probe through triazole nitrogen and catechol oxygen atoms. In contrast, coordination of **BODIPY-OO** with the  $\text{Hg}^{2+}$  changed the chemical shifts of neighboring protons in the binding site very slightly. As shown in Fig. 9,  $\text{H}_a$ ,  $\text{H}_e$ , and  $\text{H}_f$  at  $\delta$  8.01, 5.90, and 5.12 ppm were shifted to  $\delta$  8.03, 5.91, and 5.14 ppm, respectively. Very small changes in the  $^1\text{H}$  NMR spectra of **BODIPY-OO** upon increasing concentrations of



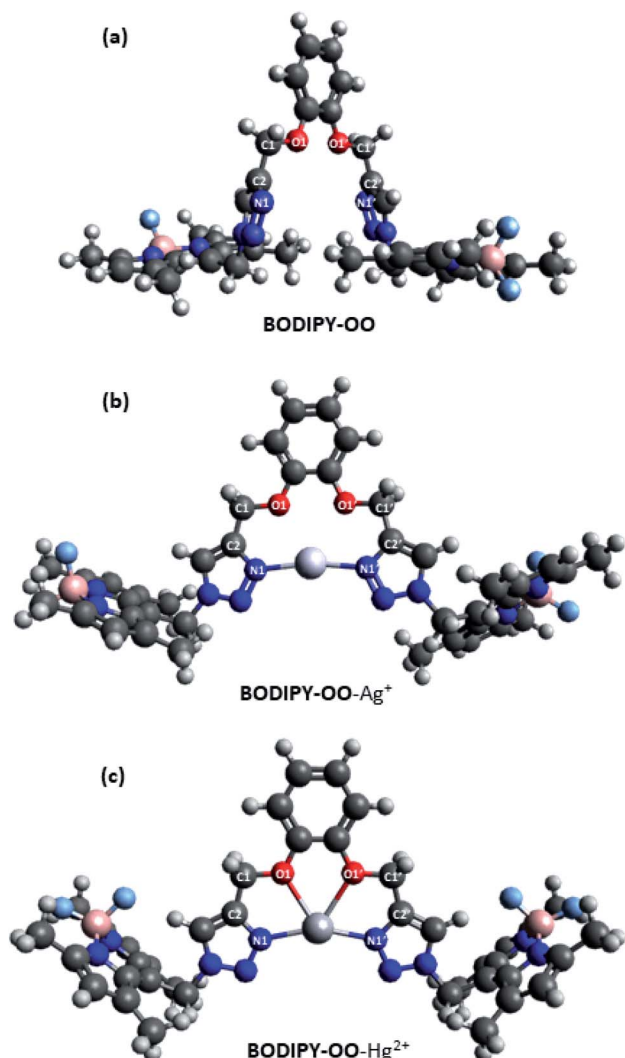


Fig. 10 Optimized structures of (a) BODIPY-OO, (b) BODIPY-OO- $\text{Ag}^+$ , and (c) BODIPY-OO- $\text{Hg}^{2+}$ .

the  $\text{Hg}^{2+}$  are possibly the effect of the rapid quadrupolar relaxation of the  $\text{Hg}^{2+}$  ion.<sup>72–74</sup>

### Theoretical calculation studies

To get insight into the mechanism on the fluorescence sensing of BODIPY-OO toward  $\text{Ag}^+$  and  $\text{Hg}^{2+}$ , density functional theory (DFT) calculations of the sensor and its complexes were

performed. Fig. 10 illustrates the calculated energy-minimized structures of BODIPY-OO, BODIPY-OO- $\text{Ag}^+$ , and BODIPY-OO- $\text{Hg}^{2+}$  complexes. It can be seen that the triazole units in the free ligand are arranged in a “face-to-face” fashion (Fig. 10a). Dihedral angles of O1-C1-C2-N1 and O1'-C1'-C2'-N1' are found nearly the same, *i.e.* 114.886° and 114.883°, respectively. On the other hand, BODIPY-OO- $\text{Ag}^+$  and BODIPY-OO- $\text{Hg}^{2+}$  complexes showed significant changes in their geometries. In Fig. 10b, the optimized geometry of BODIPY-OO- $\text{Ag}^+$  indicates that a stable complex was formed with the lone electron pairs of triazole nitrogen atoms (N1 and N1') turned toward the bound  $\text{Ag}^+$  ion. The bond lengths of N1- $\text{Ag}^+$  and N1'- $\text{Ag}^+$  were 2.19 Å, whereas the dihedral angles of O1-C1-C2-N1 and O1'-C1'-C2'-N1' were 13.734° and -9.848°, respectively. The bond angle between N1- $\text{Ag}$ -N1' of 168.77° was observed. In contrast, the optimized geometry of BODIPY-OO- $\text{Hg}^{2+}$  showed that not only N1 and N1' of the triazole rings but also O1 and O1' of the catechol unit were involved in the coordination with the  $\text{Hg}^{2+}$  center with the coordinated bond lengths of 2.22 Å (N1-Hg and N1'-Hg) and 2.48 Å (O1-Hg and O1'-Hg) (Fig. 10c). The calculated bond angle between N1-Hg-N1' was 157.83°, whereas the dihedral angles of O1-C1-C2-N1 and O1'-C1'-C2'-N1' were 0.020° and 0.033°, respectively. These results suggested that two coordinated nitrogens are not exactly linear and two triazole rings are almost in the same plane.

Furthermore, calculated frontier molecular orbitals (FMOs) of BODIPY-OO and its complexes are shown in Table S2, ESI,† and their calculated absorption data are summarized in Table 2. The main transition of BODIPY-OO was at 442 nm ( $\lambda_{\text{exp}} = 517$  nm) which is related to  $\pi \rightarrow \pi^*$  transition of the BODIPY units. That of BODIPY-OO- $\text{Ag}^+$  was found to be very similar at 440 nm ( $\lambda_{\text{exp}} = 517$  nm) since there were no significant changes in electronic transition energies of BODIPY-OO and BODIPY-OO- $\text{Ag}^+$ , *i.e.* 2.80 eV and 2.82 eV, respectively. In contrast, the  $\pi \rightarrow \pi^*$  transition of BODIPY-OO- $\text{Hg}^{2+}$  was observed at 456 nm ( $\lambda_{\text{exp}} = 531$  nm) which was red-shifted with respect to that of BODIPY-OO and BODIPY-OO- $\text{Ag}^+$  as a result of the lower energy transition (2.72 eV). These theoretical results are in good agreement with the experimental spectra. On the other hand, comparing with BODIPY-OO- $\text{Ag}^+$ , the lower energies of the HOMOs of BODIPY-OO- $\text{Hg}^{2+}$  can be ascribed to a weaker electrostatic repulsion between the metal electrons and lone electron pairs of the triazole and catechol ligands directed toward the metal center.

Notably, the electron density in FMOs of the sensor and its complexes was distributed almost only over the BODIPY units.

Table 2 Calculated electronic transition energies and oscillator strengths of BODIPY-OO, BODIPY-OO- $\text{Ag}^+$ , and BODIPY-OO- $\text{Hg}^{2+}$

| Compound                    | $\lambda_{\text{abs}}^{\text{max}}$ (nm) | Band assignment   | Excitation energy (eV) | Oscillator strength |
|-----------------------------|--|---|------------------------|---------------------|
| BODIPY-OO                   | 442                                      | H-0 $\rightarrow$ L+0 (49%)   | 2.80                   | 1.21                |
| BODIPY-OO- $\text{Ag}^+$    | 440                                      | H-1 $\rightarrow$ L+1 (49%)<br>H-0 $\rightarrow$ L+1 (57%)                                | 2.82                   | 1.08                |
| BODIPY-OO- $\text{Hg}^{2+}$ | 456                                      | H-1 $\rightarrow$ L+0 (41%)<br>H-0 $\rightarrow$ L+1 (49%)<br>H-1 $\rightarrow$ L+0 (49%) | 2.72                   | 1.17                |





In other words, the HOMO and the LUMO are heavily biased to the BODIPY units and receive only very minor contributions from the coordination center. As a consequence, the relevant excitation is adequately described as a BODIPY-based  $\pi \rightarrow \pi^*$  transition with significantly no charge-transfer contributions from the triazole fragments. Therefore, mechanisms like intramolecular charge transfer (ICT) and photoinduced electron transfer (PET) were ruled out.

## Conclusions

We have synthesized a new bifunctional chemosensor **BODIPY-OO** that can be used as a “turn-on” fluorescent probe for dual detection of  $\text{Hg}^{2+}$  and  $\text{Ag}^+$  ions. **BODIPY-OO** can clearly distinguish  $\text{Hg}^{2+}$  from  $\text{Ag}^+$  by the use of an EDTA. Modifications to chelating sites of this bis-BODIPY linked-triazole platform can not only bring more sensing information but also efficient differentiation of multiple analytes.

## Conflicts of interest

There are no conflicts to declare.

## Acknowledgements

This work was supported by the Faculty of Science, Mahidol University and the Center of Excellence for Innovation in Chemistry (PERCH-CIC), Ministry of Higher Education, Science, Research and Innovation. WS acknowledges the Science Achievement Scholarship of Thailand (SAST) for his scholarship. Finally, the authors would like to thank Assoc. Prof. Panida Surawatanawong and Mr Phiphop Naweephattana for their helpful advice and supports on DFT calculations.

## Notes and references

- 1 M. Jaishankar, T. Tseten, N. Anbalagan, B. B. Mathew and K. N. Beeregowda, *Interdiscip. Toxicol.*, 2014, **7**, 60–72.
- 2 P. C. Nagajyoti, K. D. Lee and T. V. M. Sreekanth, *Environ. Chem. Lett.*, 2010, **8**, 199–216.
- 3 Z. Xu, S. J. Han, C. Lee, J. Yoon and D. R. Spring, *Chem. Commun.*, 2010, **46**, 1679–1681.
- 4 G. Guzzi and C. A. M. La Porta, *Toxicology*, 2008, **244**, 1–12.
- 5 O. R. Luca and A. Q. Fenwick, *J. Photochem. Photobiol., B*, 2015, **152**, 26–42.
- 6 R. A. Bernhoft, *J. Environ. Health*, 2012, **2012**, 460508.
- 7 K. M. Rice, E. M. Walker, Jr, M. Wu, C. Gillette and E. R. Blough, *J. Prev. Med. Public Health*, 2014, **47**, 74–83.
- 8 Y. Zhuang, J. S. Thompson, C. J. Zygarlicke and J. H. Pavlish, *Environ. Sci. Technol.*, 2004, **38**, 5803–5808.
- 9 I. R. Gould, J. R. Lenhard, A. A. Muentner, S. A. Godleski and S. Farid, *J. Am. Chem. Soc.*, 2000, **122**, 11934–11943.
- 10 W. Shen, J. Tang, Y. Wang, J. Liu, L. Huang, W. Chen, L. Yang, W. Wang, Y. Wang, R. Yang, J. Yun and L. A. Belfiore, *ACS Appl. Mater. Interfaces*, 2017, **9**, 5358–5365.
- 11 S. Prabhu and E. K. Poullose, *Int. Nano Lett.*, 2012, **2**, 32.
- 12 J. Hards, H. Ahrens, C. Gebert, A. Streitbuerger, H. Buerger, M. Erren, A. Gunsels, C. Wedemeyer, G. Saxler, W. Winkelmann and G. Gosheger, *Biomaterials*, 2007, **28**, 2869–2875.
- 13 M. B. Gumpu, S. Sethuraman, U. M. Krishnan and J. B. B. Rayappan, *Sens. Actuators, B*, 2015, **213**, 515–533.
- 14 S.-j. Yu, Y.-g. Yin and J.-f. Liu, *Environ. Sci.: Processes Impacts*, 2013, **15**, 78–92.
- 15 B. C. Mondal, D. Das and A. K. Das, *Anal. Chim. Acta*, 2001, **450**, 223–230.
- 16 Y.-T. Li, S.-J. Jiang and A. C. Sahayam, *Food Anal. Method.*, 2017, **10**, 434–441.
- 17 M. Hosoba, K. Oshita, R. K. Katarina, T. Takayanagi, M. Oshima and S. Motomizu, *Anal. Chim. Acta*, 2009, **639**, 51–56.
- 18 X.-B. Zhang, Z.-X. Han, Z.-H. Fang, G.-L. Shen and R.-Q. Yu, *Anal. Chim. Acta*, 2006, **562**, 210–215.
- 19 A. Promchat, K. Wongravee, M. Sukwattanasinitt and T. Praneenarat, *Sci. Rep.*, 2019, **9**, 10390.
- 20 A. Kathiravan, A. Gowri, T. Khamrang, M. D. Kumar, N. Dhenadhayalan, K.-C. Lin, M. Velusamy and M. Jaccob, *Anal. Chem.*, 2019, **91**, 13244–13250.
- 21 M. Saleem, M. Rafiq and M. Hanif, *J. Fluoresc.*, 2017, **27**, 31–58.
- 22 K. P. Carter, A. M. Young and A. E. Palmer, *Chem. Rev.*, 2014, **114**, 4564–4601.
- 23 S. Voutsadaki, G. K. Tsikalas, E. Klontzas, G. E. Froudakis and H. E. Katerinopoulos, *Chem. Commun.*, 2010, **46**, 3292–3294.
- 24 L. Jin, M. Xu, H. Jiang, W. Wang and Q. Wang, *Anal. Methods*, 2018, **10**, 4562–4569.
- 25 K. Bera, A. K. Das, M. Nag and S. Basak, *Anal. Chem.*, 2014, **86**, 2740–2746.
- 26 Y. Liu, Z. Li, L. Chen and Z. Xie, *Dyes Pigm.*, 2017, **141**, 5–12.
- 27 G. Ulrich, R. Ziessel and A. Harriman, *Angew. Chem., Int. Ed.*, 2008, **47**, 1184–1201.
- 28 A. Loudet and K. Burgess, *Chem. Rev.*, 2007, **107**, 4891–4932.
- 29 K. Velmurugan, A. Raman, S. Easwaramoorthi and R. Nandhakumar, *RSC Adv.*, 2014, **4**, 35284–35289.
- 30 H. Liu, Y. Tan, Q. Dai, H. Liang, J. Song, J. Qu and W.-Y. Wong, *Dyes Pigm.*, 2018, **158**, 312–318.
- 31 Q. Lai, Q. Liu, Y. He, K. Zhao, C. Wei, L. Wojtas, X. Shi and Z. Song, *Org. Biomol. Chem.*, 2018, **16**, 7801–7805.
- 32 M. Vedamalai, D. Kedaria, R. Vasita, S. Mori and I. Gupta, *Dalton Trans.*, 2016, **45**, 2700–2708.
- 33 J. J. Bryant and U. H. F. Bunz, *Chem.-Asian J.*, 2013, **8**, 1354–1367.
- 34 M. Zurro and O. G. Mancheño, *Chem. Rec.*, 2017, **17**, 485–498.
- 35 K. Rajavelu, M. Subaraja and P. Rajakumar, *New J. Chem.*, 2018, **42**, 3282–3292.
- 36 A. I. Germeroth, J. R. Hanna, R. Karim, F. Kundel, J. Lowther, P. G. N. Neate, E. A. Blackburn, M. A. Wear, D. J. Campopiano and A. N. Hulme, *Org. Biomol. Chem.*, 2013, **11**, 7700–7704.
- 37 Y. Ling, Z.-X. Chen, F.-P. Zhai, Y.-M. Zhou, L.-H. Weng and D.-Y. Zhao, *Chem. Commun.*, 2011, **47**, 7197–7199.



- 38 R. S. Singh, R. K. Gupta, R. P. Paitandi, A. Misra and D. S. Pandey, *New J. Chem.*, 2015, **39**, 2233–2239.
- 39 A. N. Kursunlu, M. Ozmen and E. Güler, *J. Fluoresc.*, 2019, **29**, 1321–1329.
- 40 A. N. Kursunlu, *RSC Adv.*, 2015, **5**, 41025–41032.
- 41 A. N. Kursunlu and E. Güler, *J. Mol. Struct.*, 2017, **1134**, 345–349.
- 42 X. Liu, X. Yang, H. Peng, C. Zhu and Y. Cheng, *Tetrahedron Lett.*, 2011, **52**, 2295–2298.
- 43 S. Y. Lee, K. H. Bok and C. Kim, *RSC Adv.*, 2017, **7**, 290–299.
- 44 S. Khatua and M. Schmittel, *Org. Lett.*, 2013, **15**, 4422–4425.
- 45 X. Zhang, Y. Xu, P. Guo and X. Qian, *New J. Chem.*, 2012, **36**, 1621–1625.
- 46 J. H. Brannon and D. Magde, *J. Phys. Chem.*, 1978, **82**, 705–709.
- 47 F. Heisig, S. Gollos, S. J. Freudenthal, A. El-Tayeb, J. Iqbal and C. E. Müller, *J. Fluoresc.*, 2014, **24**, 213–230.
- 48 M. J. Frisch, G. W. Trucks, H. B. Schlegel, G. E. Scuseria, M. A. Robb, J. R. Cheeseman, G. Scalmani, V. Barone, B. Mennucci, G. A. Petersson, H. Nakatsuji, M. Caricato, X. Li, H. P. Hratchian, A. F. Izmaylov, J. Bloino, G. Zheng, J. L. Sonnenberg, M. Hada, M. Ehara, K. Toyota, R. Fukuda, J. Hasegawa, M. Ishida, T. Nakajima, Y. Honda, O. Kitao, H. Nakai, T. Vreven, J. A. Montgomery Jr., J. E. Peralta, F. Ogliaro, M. Bearpark, J. J. Heyd, E. Brothers, K. N. Kudin, V. N. Staroverov, T. Keith, R. Kobayashi, J. Normand, K. Raghavachari, A. Rendell, J. C. Burant, S. S. Iyengar, J. Tomasi, M. Cossi, N. Rega, J. M. Millam, M. Klene, J. E. Knox, J. B. Cross, V. Bakken, C. Adamo, J. Jaramillo, R. Gomperts, R. E. Stratmann, O. Yazyev, A. J. Austin, R. Cammi, C. Pomelli, J. W. Ochterski, R. L. Martin, K. Morokuma, V. G. Zakrzewski, G. A. Voth, P. Salvador, J. J. Dannenberg, S. Dapprich, A. D. Daniels, Ö. Farkas, J. B. Foresman, J. V. Ortiz, J. Cioslowski and D. J. Fox, *Gaussian 09, Revision C.01*, Gaussian, Inc., Wallingford CT, 2010.
- 49 C. Lee, W. Yang and R. G. Parr, *Phys. Rev. B: Condens. Matter Mater. Phys.*, 1988, **37**, 785–789.
- 50 A. D. Becke, *J. Chem. Phys.*, 1993, **98**, 5648–5652.
- 51 P. C. Hariharan and J. A. Pople, *Theor. Chim. Acta*, 1973, **28**, 213–222.
- 52 G. A. Petersson, A. Bennett, T. G. Tensfeldt, M. A. Al-Laham, W. A. Shirley and J. Mantzaris, *J. Chem. Phys.*, 1988, **89**, 2193–2218.
- 53 P. J. Hay and W. R. Wadt, *J. Chem. Phys.*, 1985, **82**, 270–283.
- 54 W. R. Wadt and P. J. Hay, *J. Chem. Phys.*, 1985, **82**, 284–298.
- 55 P. J. Hay and W. R. Wadt, *J. Chem. Phys.*, 1985, **82**, 299–310.
- 56 T. Yanai, D. P. Tew and N. C. Handy, *Chem. Phys. Lett.*, 2004, **393**, 51–57.
- 57 V. Barone and M. Cossi, *J. Phys. Chem. A*, 1998, **102**, 1995–2001.
- 58 M. Cossi, N. Rega, G. Scalmani and V. Barone, *J. Comput. Chem.*, 2003, **24**, 669–681.
- 59 *Avogadro: an open-source molecular builder and visualization tool. Version 1.2.0*, <http://avogadro.cc/>.
- 60 M. D. Hanwell, D. E. Curtis, D. C. Lonie, T. Vandermeersch, E. Zurek and G. R. Hutchison, *J. Cheminf.*, 2012, **4**, 17.
- 61 H. Lu, J. Mack, Y. Yang and Z. Shen, *Chem. Soc. Rev.*, 2014, **43**, 4778–4823.
- 62 I. T. Ho, T.-L. Lai, R.-T. Wu, M.-T. Tsai, C.-M. Wu, G.-H. Lee and W.-S. Chung, *Analyst*, 2012, **137**, 5770–5776.
- 63 D.-T. Shi, X.-L. Wei, Y. Sheng, Y. Zang, X.-P. He, J. Xie, G. Liu, Y. Tang, J. Li and G.-R. Chen, *Sci. Rep.*, 2014, **4**, 4252.
- 64 Z. Shi, X. Han, W. Hu, H. Bai, B. Peng, L. Ji, Q. Fan, L. Li and W. Huang, *Chem. Soc. Rev.*, 2020, **49**, 7533–7567.
- 65 H.-C. Hung, C.-W. Cheng, Y.-Y. Wang, Y.-J. Chen and W.-S. Chung, *Eur. J. Org. Chem.*, 2009, **2009**, 6360–6366.
- 66 J. Fan, C. Chen, Q. Lin and N. Fu, *Sens. Actuators, B*, 2012, **173**, 874–881.
- 67 W. Shi, Y. Chen, X. Chen, Z. Xie and Y. Hui, *J. Lumin.*, 2016, **174**, 56–62.
- 68 B. Sen, M. Mukherjee, S. Banerjee, S. Pal and P. Chattopadhyay, *Dalton Trans.*, 2015, **44**, 8708–8717.
- 69 V. S. Jisha, A. J. Thomas and D. Ramaiah, *J. Org. Chem.*, 2009, **74**, 6667–6673.
- 70 Y. Zhang, X. Li, L. Gao, J. Qiu, L. Heng, B. Z. Tang and L. Jiang, *ChemPhysChem*, 2014, **15**, 507–513.
- 71 D. C. Harris, *Quantitative Chemical Analysis*, W.H. Freeman and Company, New York, 2010.
- 72 J. Kronenbitter, U. Schweizer and A. Schwenk, *Z. Naturforsch.*, 1980, **35**, 319.
- 73 R. E. Wasylshen, R. E. Lenkinski and C. Rodger, *Can. J. Chem.*, 1982, **60**, 2113–2117.
- 74 M. Maliarik and I. Persson, *Magn. Reson. Chem.*, 2005, **43**, 835–842.

